DOI: 10.13009/EUCASS2022-4404
9TH EUROPEAN CONFERENCE FOR AERONAUTICS AND SPACE SCIENCES (EUCASS)

Advanced Aircraft Braking Control Laws Design and Validation

Amath Waly Ndiaye[⋆□†], *Jean-Marc Biannic*[⋆], *Mario Cassaro*[⋆], *Clément Combier*[□] *and Jean-Baptiste Lestage*[□]
[⋆]*Onera - The French Aerospace Lab, 31055 Toulouse, France*
[□]*Safran Landing Systems, 78140 Vélizy-Villacoublay, France*
[†]amath-waly.ndiaye@safrangroup.com

Abstract

Aircraft anti-skid controllers rely still mostly on heuristic wheel deceleration-based strategies despite the recent advances made in automotive applications. This paper presents a novel aircraft braking control design method which unlocks all the wheel slip control benefits for aeronautics. Based on a simple synthesis model, a wheel slip controller is derived, its gains being scheduled to adapt to the varying system dynamics. An extended state observer is then used to provide accurate estimations of the wheel grip moment and slip. Robustness and performance of the proposed approach are finally demonstrated through simulations on a realistic validation model.

1. Introduction

Despite the recent enhancement of aircraft on-ground control, anti-skid braking systems remain today mostly heuristic algorithms focused on confining the wheel deceleration within empirical thresholds[1,2] . Although such strategies rely only on the wheel speed and braking pressure measurements, they lack generality, require tedious tuning procedures and may be sub-optimal. Recent advances for automotive applications[3,4] introduced novel wheel slip-based control strategies able to achieve better performance and robustness for a reduced tuning effort. However, those ABS solutions cannot be directly transferred to aircraft for multiple reasons. A major one is the unavailability of the aircraft velocity measure to the braking control unit (BCU) for the sake of safety and modularity[5] . Besides limited measurements access, an aircraft antiskid control system has also more stringent requirements in a wider operating range. Mass variations, runway conditions and carbon brake gain fluctuations make the control design phase a challenging problem. In addition, the recent efforts to reduce the ground piloting workload introduced development of advanced control functions, *e.g.* automatic taxi-guidance[6,7] , which could be further improved by means of modern braking strategies able to perform efficient automatic braking (*autobrake*). In that respect, to unlock all the potential benefits of slip control in aeronautics, a real challenge consists in designing robust, high-performing and generic wheel slip control laws that rely only on the landing gear common set of sensors, namely the braking pressure transducer and wheel speedometer.[8] Leveraging the key results regarding tire friction force and wheel slip estimation[9,10] , recent studies adapted active braking control strategies to aeronautics by using a combination of wheel slip and deceleration as the controlled variable.[11,12] At the expense of an additional tuning parameter, such an approach takes advantage of the wheel speed measurement reliability, and thus mitigates the effects of slip estimation error and noise sensitivity arising at low speeds. Several studies used neural networks and fuzzy-logic for the anti-skid[13,14] , however the certification of such approaches may be difficult due to the high level of reliability expected by aviation authorities. Furthermore, a neural network-based estimator for wheel slip may not offer better results than model-based observers[8] . Model Predictive Control was also investigated with considerations on how to reduce the inherent computational load of the optimization resolution occurring at each time step[15] . Due to the slip control intrinsic noise amplification, particularly for low speed and slip setpoint values, it appears important to design low order controllers, thus limiting the control signal noise sensitivity. Moreover, designing an effective solution, easily tunable and adaptable, as well as realistic in terms of computing power and certification issues, is highly desirable for landing gear manufacturers.
The proposed research aims to develop a wheel slip control architecture implementable in current aircraft landing gear layout thanks to an efficient wheel slip estimation method. The contribution of this paper is twofold:

1. A novel slip control law is designed to cover the entire operating range of the system by combining a scheduled PI controller, active in the stable region of the friction curve, with a nonlinear dynamic inversion (NDI) controller used to cope with slip values beyond the friction peak. Actuator dynamics and sensor delays are accounted for in the design process leading to realistic limitations on the achievable performance.

DOI: 10.13009/EUCASS2022-4404

2. An efficient extended state observer (ESO) is conceived to reconstruct the wheel grip moment, the aircraft speed and the wheel slip. The system nonlinearity being inherent to the grip moment, this exhaustive estimation approach allows to obtain accurate estimates over the whole operating domain but also to perform nonlinear compensation.

In that respect, the proposed work allows direct implementation of a generic advanced braking control architecture on aircraft with the current landing gear limited set of measurements commonly available. The complete approach is validated through simulation on a high-fidelity/medium complexity aircraft model previously proposed by the authors.[16]

The paper is organized as follows: section 2 introduces a simplified single wheel model employed for control synthesis. The switching control law is derived in section 3. Section 4 presents the extended state observer used to estimate the wheel grip moment, from which the aircraft speed and wheel slip estimates are deducted. Performance and robustness of the control strategy are demonstrated in section 5 via simulations on the validation model, depicting meaningful critical braking conditions.

2. Problem objectives and formulation

The objective of the proposed research is to derive a novel wheel slip control scheme for aeronautic application with advanced functionalities, *e.g. autobrake*, meeting the safety requirements by mitigating wheel skids and able to efficiently track a slip setpoint in the stable region of the friction curve. The only measurements assumed available are the commanded torque, *i.e.* the control signal, and the wheel rotational speed.

2.1 Synthesis model

The mathematical model used for controller design is a simple single wheel model, also referred to as a quarter car model in the automotive context[3] . As depicted in Figure 1, it consists of a wheel attached to a mass m for which only the longitudinal motion is considered. The wheel is in contact with the runway, assumed perfectly horizontal. The aerodynamic drag is neglected for control design but will be taken into account in sections 4 and 5 for estimation purposes and the validation of the control architecture on the high-fidelity aircraft model.

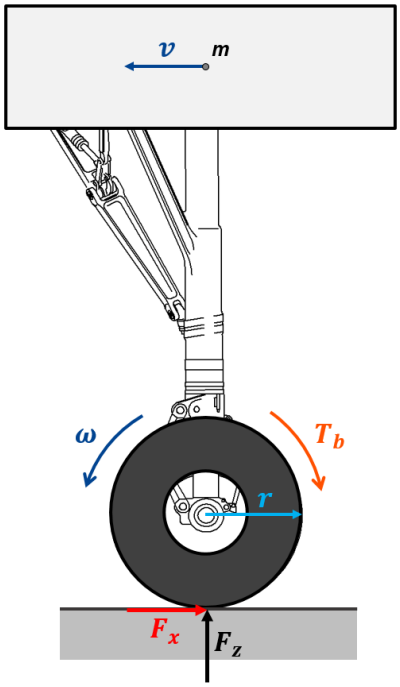

Figure 1: Single wheel model

The single wheel model equations of motion can be written as:

DOI: 10.13009/EUCASS2022-4404

$$m\dot{v} = -F_x \tag{1}$$

$$J\dot{\omega} = rF_x - T_b \tag{2}$$

where v, ω, J,and r are the longitudinal velocity, wheel rotational speed, inertia and rolling radius respectively, as in Figure 1. T_b represents the braking torque and is the control variable of the problem. F_z and F_x are the vertical load and tire longitudinal friction force respectively, the latter being given by:

$$F_x = F_z\,\mu(\lambda) \tag{3}$$

where $\mu(\lambda)$ is the friction characteristic of the tire/runway interface. This friction coefficient depends mainly on the wheel longitudinal slip λ defined as:

$$\lambda = \frac{v - r\omega}{v} \tag{4}$$

One can notice that the value of λ remains between 0, corresponding to an unbraked rolling wheel, and 1, reached when the wheel is locked. Typical friction characteristics $\mu(\lambda)$ are displayed in Figure 2. It should be mentioned that other parameters, like the velocity v or the vertical load F_z, have an influence on these friction curves, see Pacejka.[17]

As in Johansen et al.,[4] (2) and (4) can be combined to reformulate the problem in a wheel slip-dependent fashion:

$$\dot{\lambda} = -\frac{r}{Jv}\left(1 + \frac{J}{mr^2}(1-\lambda)\right)\Psi(\lambda) + \frac{r}{Jv}T_b \tag{5a}$$

$$\dot{v} = -\frac{1}{m}F_z\mu(\lambda) \tag{5b}$$

where we denoted by Ψ the wheel grip moment defined as:

$$\Psi(\lambda) = r\,F_z\,\mu(\lambda) \tag{6}$$

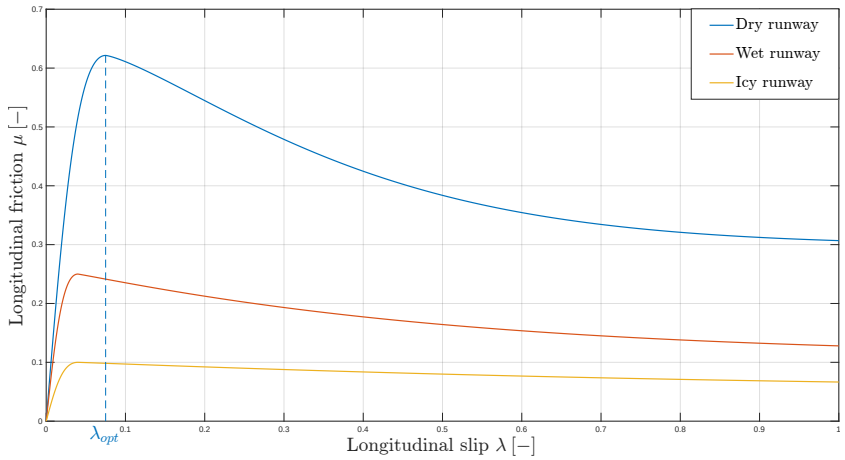

Figure 2: Tire friction characteristics $\mu(\lambda)$ for different runway conditions

Considering that, for an aircraft, the wheel inertia J is much smaller than the equivalent mass m, the term $\frac{J}{mr^2}$ is negligible in comparison with 1, and (5a) can be written as:

$$\dot{\lambda} \approx \frac{r}{Jv}\Big(T_b - \Psi(\lambda)\Big) \tag{7}$$

As can be seen in Figure 2, the friction μ is a nonlinear function of λ, characterized by a maximum value corresponding to an optimal slip λ_{opt} (displayed for the dry condition only). After linearization around an equilibrium point $(\bar{\lambda}, \bar{v})$, see Savaresi et al,[3] Castro et al[18] for further details, (7) becomes:

$$\dot{\delta}_\lambda = \frac{r}{J\bar{v}}\Big(\delta_{T_b} - \gamma(\bar{\lambda})\delta_\lambda\Big) \tag{8}$$

DOI: 10.13009/EUCASS2022-4404

where δ_λ and δ_{T_b} represent the variations around the equilibrium point values $\bar{\lambda}$ and $\bar{T}_b$ respectively. $\gamma(\lambda)$ is the derivative of the grip moment with respect to the slip, and is proportional to the friction curve slope according to:

$$\gamma(\lambda) = r\, F_z\, \frac{\partial \mu}{\partial \lambda}(\lambda) \tag{9}$$

The evolution of $\gamma(\lambda)$ for the dry runway friction of Figure 2 is represented in Figure 3, where a linear approximation of the curve over the stable region is also plotted for the domain $\lambda \in [0,\ \lambda_{opt}]$.

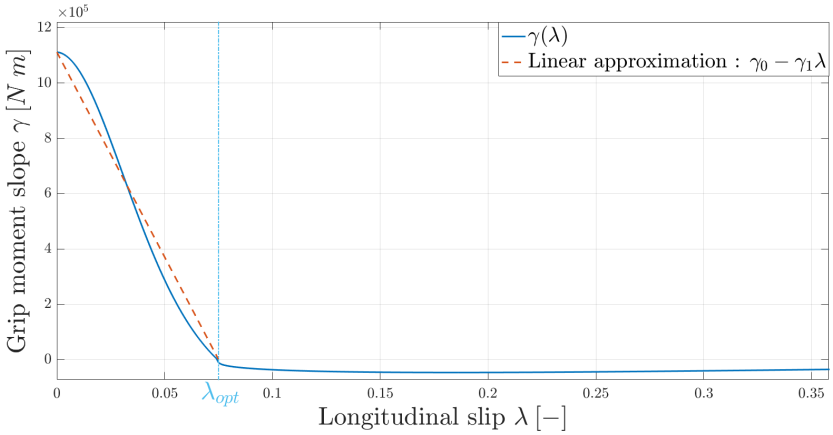

Figure 3: Evolution of the grip moment slope $\gamma(\lambda)$ for a dry runway

Considering (8), the first-order transfer function of the single wheel model, from brake torque to wheel slip, finally reads as follows:

$$G_{\bar{\lambda}}(s) = \frac{\frac{r}{J\bar{v}}}{s + \frac{r}{J\bar{v}}\gamma(\bar{\lambda})} \tag{10}$$

Note that the system is unstable for negative values of γ, *i.e.* for $\bar{\lambda} > \lambda_{opt}$, where the real pole is positive.

Remarks. *As can be seen in Figure 3, for a dry runway, γ experience significant variations , from $60\,kN\,m$ to $0\,N\,m$ on the stable region ($\gamma > 0$). Let us write p_0, G_0 and G_∞ the pole, static and high-frequency gains of the open loop transfer function $G_{\bar{\lambda}}(s)$ respectively. The study of its behavior for the operating conditions $\bar{\lambda} \in [0, 1]$ and $\bar{v} \in]0, 70]$ allows to notice the following:*

- *at low velocity ($\bar{v} \to 0$), we have $|p_0| \to \infty$ and $G_\infty \to \infty$, which means the wheel slip dynamics becomes extremely fast (i.e. uncontrollable considering the actuator bandwidth and wheel skids are quasi impossible to counter) while noise sensitivity is amplified. That is why antiskid systems are usually turned off below approximately $10\,m/s$. These impediments are well known in the automotive industry, but the inability to counter low velocity skids is all the more obvious in an aeronautic context given the substantial values of F_z. To tackle this $\bar{v}$-dependency, a gain-scheduling strategy applied all along the braking process appears relevant as previously done in Johansen et al,[4] Castro et al.[18]*

- *For large values of γ, i.e. very small λ, we have $-p_0 \gg 0$ and $G_0 \ll 1$, while when approaching λ_{opt}, $p_0 \to 0$ and $G_0 \to 0$. The system is dramatically fast on most of the stable region of the friction curve, whereas its time constant increases considerably near the friction peak. Meanwhile, the slip variation for a given increase of T_b is also amplified near λ_{opt}. Based on this analysis, changing the system dynamics in the stable very fast region is irrelevant. The required control law should rather confer a faster stable pole in the vicinity of the friction peak, i.e. where the antiskid is generally activated.*

- *For $\lambda > \lambda_{opt}$, i.e. the unstable operating domain, γ and p_0 do not vary as considerably as in the stable part with respect to λ. Though, p_0 takes significant values rapidly, the system being unstable and fast.*

The hydraulic actuator bandwidth and sensor delay being non-negligible given the fast system dynamics in most of its operating range, both have to be taken into account for closed loop analysis.

Electro-hydraulic servo-valve actuators can be accurately modeled by second order transfer functions[19] . Based on experimental and manufacturing data, the following model is retained for the actuator dynamics:

DOI: 10.13009/EUCASS2022-4404

$$A(s) = \frac{\omega_0^2}{s^2 + 2\xi\omega_0\, s + \omega_0^2} \tag{11}$$

with $\omega_0 \approx 30\, rad/s$ and $\xi \approx 0.6$ the natural frequency and damping ratio, respectively.

The wheel speedometer is processed using a fixed-position estimator, as in Brown et al[20] . The resulting speed measurement is delayed with respect to the real wheel speed ω. This delay is due to both the sampling period T_s, generating a constant lag time $\frac{T_s}{2}$, and the speedometer finite resolution (number of teeth N), introducing a velocity-dependent term:

$$d_\omega(\omega) = \frac{\frac{2\pi}{N}}{\omega} + \frac{T_s}{2} \tag{12}$$

In the present case, the values $N = 100$ and $T_s = 7\, ms$ characterize the wheel speed measurement delay. As such, the conservative constant value $d_\omega = 5ms$, corresponding to the rather unfavorable low velocity $\omega \approx 30\, rad/s$, is retained for closed-loop preliminary analysis and observer design (sections 2.2 and 4 respectively). This constant delay transfer function can be modeled by a Padé approximation:

$$S(s) = \frac{1 - \frac{d_\omega}{2} s}{1 + \frac{d_\omega}{2} s} \tag{13}$$

For validation purpose, the aircraft model previously proposed by the authors[16] will be supplemented by the speedometer dynamic delay model (12).

2.2 Preliminary closed loop analysis

Let us consider a PI controller $K(s) = K_p + \frac{K_i}{s}$ for the system. Without actuator dynamics and sensor delay, the following second order characteristic equation is obtained from (8):

$$s^2 + \frac{r}{J\bar{v}}\left(K_p + \gamma(\bar{\lambda})\right) s + \frac{r}{J\bar{v}} K_i = 0 \tag{14}$$

A desired uniform closed-loop behavior characterized by natural frequency ω_d and damping ξ_d can, a priori, be obtained by choosing the integral and proportional gains K_i and K_p as follows:

$$K_i = \frac{J\bar{v}}{r}\omega_d^2 \tag{15a}$$

$$K_p = -\gamma(\bar{\lambda}) + 2\frac{J\bar{v}}{r}\xi_d\, \omega_d \tag{15b}$$

Such control action would in fact be equivalent to compensating the nonlinearity $\Psi(\lambda)$ through the term $-\gamma(\bar{\lambda})$ in K_p, and it is also referred to as nonlinear dynamic inversion (NDI). However, the term $\frac{\gamma(\lambda)r}{J\bar{v}}$ incur considerable and fast variations (see Figure 3), making the open loop system faster than the actuator.

Given (15), a preliminary closed loop analysis can show the limitations introduced by the servo-valve dynamics and speedometer delay. The closed loop containing the nonlinear single wheel model, as well as the actuator (11), sensor (13) and PI controller, as represented in Figure 4, is linearized for different values $\gamma(\bar{\lambda})$. Note that the wheel slip is assumed to be measured and delayed accordingly. A constant longitudinal velocity $\bar{v} = 40$ corresponding to a favorable case is retained. The resulting maximum real part of the closed loop poles is plotted in Figures 5 and 6 for different desired cutoff frequencies ω_d (see (15)) and operating points $\gamma(\bar{\lambda})$, so as to detect instability.

As can be seen in Figure 5, even for positive γ, with the designed controller, the closed loop is unstable. A uniform behavior, even over the open-loop stable subdomain $\gamma > 0$, is not achievable with a PI controller since the system dynamics incur considerable changes, from significantly faster to slower than the actuator. Figure 6 shows that the unstable region is not stabilized by the controller, in fact, in most of the domain where $\gamma < 0$, the open loop unstable pole p_0 is considerably fast and the system cannot be stabilized considering the actuator dynamics and sensor delay. More generally, the significant variations incurred by the system are faster than the actuator bandwidth in most of the domain, which leads to an imperfect compensation of the nonlinear term $\Psi(\lambda)$. Thus, a uniform behavior cannot be achieved.

DOI: 10.13009/EUCASS2022-4404

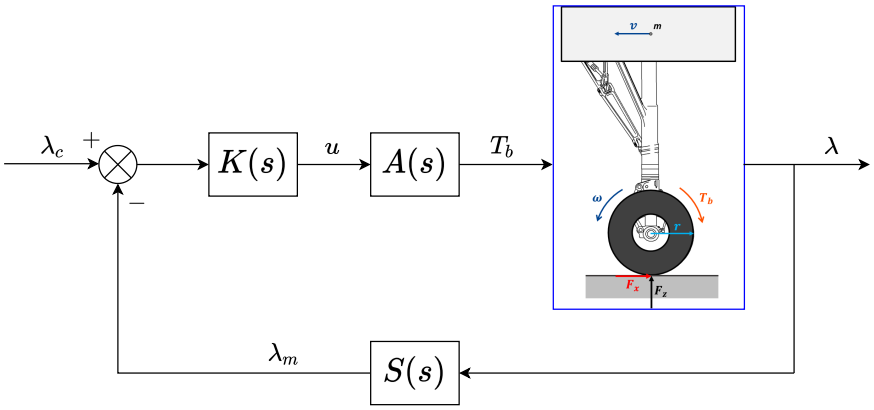

Figure 4: Closed loop block diagram ($K(s)$ given in (15))

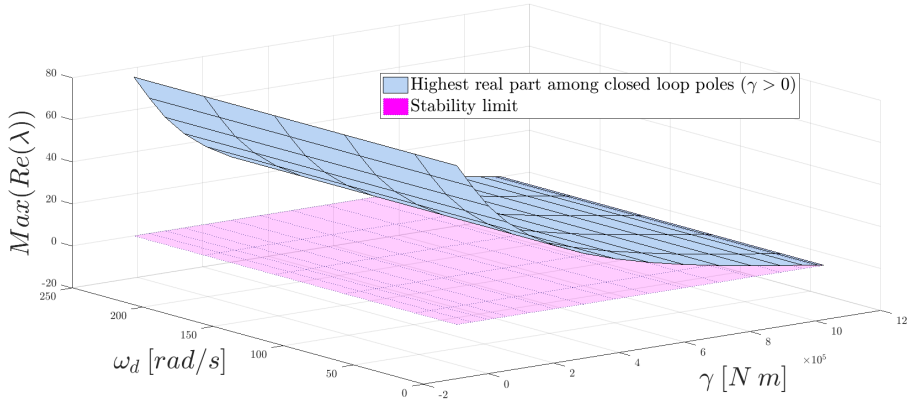

Figure 5: Evolution of the highest real part value among closed loop poles ($\gamma > 0$, K_p and K_i given in (15))

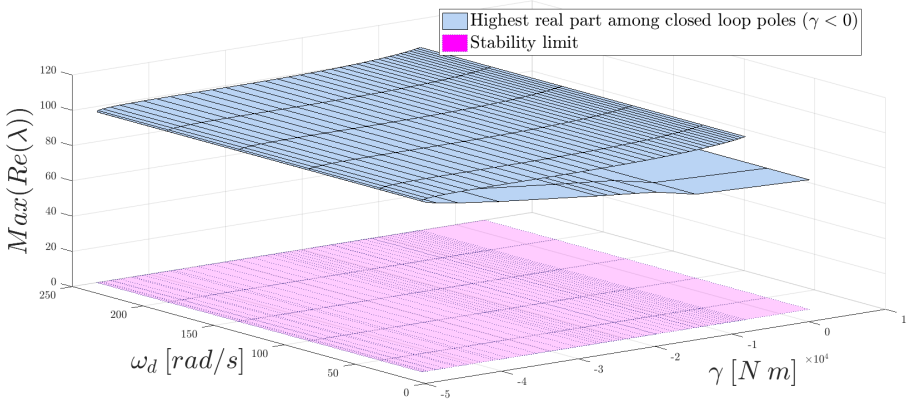

Figure 6: Evolution of the highest real part value among closed loop poles: the closed loop remains unstable $\forall\ \gamma \leq 0$ and (K_p, K_i) given in (15)

DOI: 10.13009/EUCASS2022-4404

This preliminary study showed the main difficulties of the problem arising from the strong nonlinearity of the tire/runway friction characteristic. Given the drastic changes in system dynamics and the non negligible actuator bandwidth and sensor delay, the closed loop behavior displays serious limitations. A uniform closed loop dynamics over the entire operating domain is impossible to attain with a low order controller. However, it should be more relevant to focus on conferring a desired behavior in the vicinity of the friction peak, where the actuator has sufficient bandwidth with respect to the system dynamics ($p_0 \to 0$). Moreover, given the impossibility to stabilize the unstable region, a suitable strategy to leave this domain and retrieve the stable configuration is needed.

3. Wheel slip control

3.1 Stable region scheduled PI controller

As confirmed by the preliminary analysis performed in 2.2, a low order controller can have a meaningful impact on the system poles only in the vicinity of the friction peak. In fact, a uniform behavior cannot be obtained over the whole possible values of λ, and this is also true for the subdomain $\lambda < \lambda_{opt}$. This subsection deals with the stable domain of the friction curve, which is characterized by wheel slip values below the friction peak, *i.e.* $\lambda < \lambda_{opt}$.
Let us consider the following PI control action, given the setpoint λ_c assumed not far from λ_{opt}, while neglecting in the first instance the actuator dynamics and sensor delay:

$$T_b = K_p(v)\,(\lambda_c - \lambda) + \int_0^t K_i(\lambda(\tau), v)\,(\lambda_c(\tau) - \lambda(\tau))d\tau \tag{16}$$

with $K_p(v)$ and $K_i(\lambda, v)$ assumed linear functions of v and λ and v respectively. The dynamics of the longitudinal velocity v is neglected as it varies slowly in comparison with λ.
Equation (7) allows to rewrite the system nonlinear equations:

$$\begin{cases} \dot{\lambda} = \frac{r}{Jv}\left(K_p(v)\ (\lambda_c - \lambda) - x - \Psi(\lambda)\right) = f_1(\delta_\lambda, x) \\ \dot{x} = K_i(\lambda, v)\ (\lambda - \lambda_c) = f_2(\delta_\lambda, x) \end{cases} \tag{17}$$

with $\delta_\lambda = \lambda - \lambda_c$.
Then, denoting $f = \begin{bmatrix} f_1 \\ f_2 \end{bmatrix}$ and $X = \begin{bmatrix} \delta_\lambda \\ x \end{bmatrix}$, the jacobian matrix of the system can be expressed as:

$$\frac{\partial f}{\partial X} = \begin{bmatrix} -\frac{r}{Jv}\left(K_p(v) + \gamma(\lambda)\right) & -\frac{r}{Jv} \\ K_i(\lambda, v) + \frac{\partial K_i}{\partial \lambda}\,\delta_\lambda & 0 \end{bmatrix} \tag{18}$$

From (18), the following second order characteristic equation is obtained:

$$s^2 + \frac{r}{Jv}\left(K_p(v) + \gamma(\lambda)\right)s + \frac{r}{Jv}\left(K_i(\lambda, v) + \delta_\lambda \frac{\partial K_i}{\partial \lambda}\right) = 0 \tag{19}$$

A desired closed-loop behavior, characterized by the design parameter α, can be obtained by choosing K_i and K_p such that:

$$\left(K_p(v) + \gamma(\lambda)\right)\frac{r}{Jv} = \frac{r}{Jv}\gamma(\lambda) + \alpha \tag{20a}$$

$$\frac{r}{Jv}\left(K_i(\lambda, v) + \delta\lambda\,\frac{\partial K_i}{\partial \lambda}\right) = \frac{r}{Jv}\gamma(\lambda)\,\alpha + \frac{\alpha^2}{2} \tag{20b}$$

Indeed, such gains would ensure that near the friction peak ($\gamma \approx 0$), the following poles are obtained:

$$\begin{cases} p_1 = -\frac{\alpha}{2}(1 + j) \\ p_2 = -\frac{\alpha}{2}(1 - j) \end{cases} \tag{21}$$

while when $\gamma \gg 1$:

$$\begin{cases} p_1 \approx -\frac{r}{Jv}\gamma(\lambda) \\ p_2 \approx -\alpha \end{cases} \tag{22}$$

From (20a), the gain K_p can be deduced:

$$K_p(v) = \frac{Jv}{r}\alpha \tag{23}$$

DOI: 10.13009/EUCASS2022-4404

Assuming that γ is a linear function of λ in the stable region of the friction curve:

$$\gamma(\lambda) \approx \gamma_0 - \gamma_1 \, \lambda \tag{24}$$

with γ_0 and γ_1 positive fitting coefficients ($\gamma_0 = 1.11 \times 10^6 \, Nm$ and $\gamma_1 = 1.48 \times 10^7 \, Nm$ for the dry runway in Figure 3). In that respect, the coefficients β_0 and β_1 such that $K_i(\lambda, v) = \beta_0 - \beta_1 \, \lambda$ can be determined from (20b):

$$\begin{cases} \beta_1 = \frac{1}{2} \alpha \, \gamma_1 \\ \beta_0 = \alpha \, \gamma_0 - \frac{1}{2} \alpha \, \gamma_1 \, \lambda_c + \frac{Jv}{r} \frac{\alpha^2}{2} \end{cases} \tag{25}$$

Thus, the integral gain expression can be written as:

$$K_i(\lambda, v) = \frac{\alpha}{2} \Big((\gamma_0 - \gamma_1 \, \lambda) + (\gamma_0 - \gamma_1 \, \lambda_c) \Big) + \frac{Jv}{2r} \alpha^2 = \frac{\alpha}{2} \Big(\gamma(\lambda) + \gamma(\lambda_c) \Big) + \frac{Jv}{2r} \alpha^2 \tag{26}$$

Note that since the setpoint is assumed near the optimal value λ_{opt}, we have $\gamma(\lambda_c) \approx 0$ and the integral scheduled coefficient becomes finally:

$$K_i(\lambda, v) = \frac{\alpha}{2} \left(\gamma(\lambda) + \frac{Jv}{r} \alpha \right) \tag{27}$$

The scheduled gains $K_p(v)$ and $K_i(\lambda, v)$ given by (23) and (27) allow to preserve the inherent system stability and rapidity when $\gamma \gg 1$, while they guarantee a stable, faster dynamics in the vicinity of λ_{opt}. The system linearized around any $\bar{\lambda} < \lambda_{opt}$ will verify:

$$\begin{cases} p_1 + p_2 = -\frac{r}{J\bar{v}} \gamma(\bar{\lambda}) - \alpha \\ p_1 \, p_2 = \frac{r \, \alpha}{J\bar{v}} \gamma(\bar{\lambda}) + \frac{\alpha^2}{2} \end{cases} \tag{28}$$

The design parameter α is chosen to meet, at the friction peak, the constraints regarding the actuator bandwidth, namely:

$$\omega_d(\gamma = 0) = \frac{\alpha}{\sqrt{2}} = \frac{\omega_0}{3} \tag{29}$$

which corresponds to $\alpha = 14$.

3.2 Unstable region NDI controller

In this subsection, a controller operating in the domain characterized by $\lambda > \lambda_c$ is derived. More specifically, the proposed controller is activated as soon as the slip exceeds the setpoint λ_c by a sufficient margin (further defined in section 3.3), its objective being to bring back the slip into the domain $\lambda \leq \lambda_c$ in finite time.

Let us write t_k, the time at which the controller in question is initialized, t the current time and $\hat{\Psi}(\lambda(t))$ the best current estimate of the grip moment. We assume that the grip moment and its estimate stay both bounded by the maximum braking torque applicable $T_{b_{max}} > 0$, representing the actuator maximum capacity. In this way, the error $\Delta\Psi(\lambda(t)) = \hat{\Psi}(\lambda(t)) - \Psi(\lambda(t))$ verifies:

$$|\Delta\Psi(\lambda(t))| \leq T_{b_{max}} \quad \forall \, t \geq t_k \tag{30}$$

In order to avoid abrupt changes in the control action after switching and to ensure that the braking pressure is smoothly released until the longitudinal slip reaches the objective λ_c in the stable region, we consider the following control law:

$$T_b(t) = \hat{\Psi}(\lambda) - K \, (t - t_k) \tag{31}$$

where K is a positive constant to be tuned.

Let us initially assume that a perfect estimation of Ψ is available. In this case, (7) becomes:

$$\dot{\lambda} = -\frac{r}{Jv} K \, (t - t_k) \tag{32}$$

Recalling that v undergoes slow variations when compared to λ ($\dot{v} \ll \dot{\lambda}$) on the considered interval $[t_k, t]$, then by integration one obtains:

DOI: 10.13009/EUCASS2022-4404

$$\lambda(t) = \lambda(t_k) - \frac{r}{2Jv} K\,(t - t_k)^2 \tag{33}$$

From which we readily observe that the desired objective λ_c is reached in finite time $t_{f_{nom}}$:

$$t_{f_{nom}} = t_k + \left(\frac{2Jv}{Kr}(\lambda(t_k) - \lambda_c)\right)^{\frac{1}{2}} \tag{34}$$

which is clearly a decreasing function of K.

Remark 1. *In a worst-case configuration where the estimation error is such that:* $\forall\, t \geq t_k,\ \Delta\Psi(t) = \delta_\Psi > 0$, *the required time* $t_{f_{wc}}$ *becomes:*

$$t_{fwc} = t_k + \frac{\delta_\Psi}{K} + \left(\frac{\delta_\Psi^2}{K^2} + 2\frac{Jv}{Kr}(\lambda(t_k) - \lambda_c)\right)^{\frac{1}{2}} \tag{35}$$

and we have:

$$t_{fwc} \leq t_{f_{nom}} + 2\frac{\delta_\Psi}{K} \tag{36}$$

Remark 2. *From* (34) *and* (36)*, the benefits of a gain-scheduling approach with respect to* v *is again noticeable. Indeed, by choosing* $K(v) = \Gamma\, v$*, with* Γ *a positive design constant, the leaving time becomes insensitive to the velocity. Hence, an improvement of* (31) *is proposed as:*

$$T_b(t) = \hat{\Psi}(\lambda) - K(v)\ (t - t_k) \tag{37}$$

As a final result, the explicitly time-varying control law (37) brings the system (7) back in the safe region ($\lambda \leq \lambda_c$) in a finite time t_f, which is a decreasing function of $K(v)$.

3.3 Switching strategy

To avoid unwanted switching between the two control laws near λ_c, a positive threshold h_λ, such that $\lambda_c + h_\lambda < \lambda_{opt}$, is defined so as to introduce an hysteresis cycle in the commutation strategy as illustrated in Figure 7.

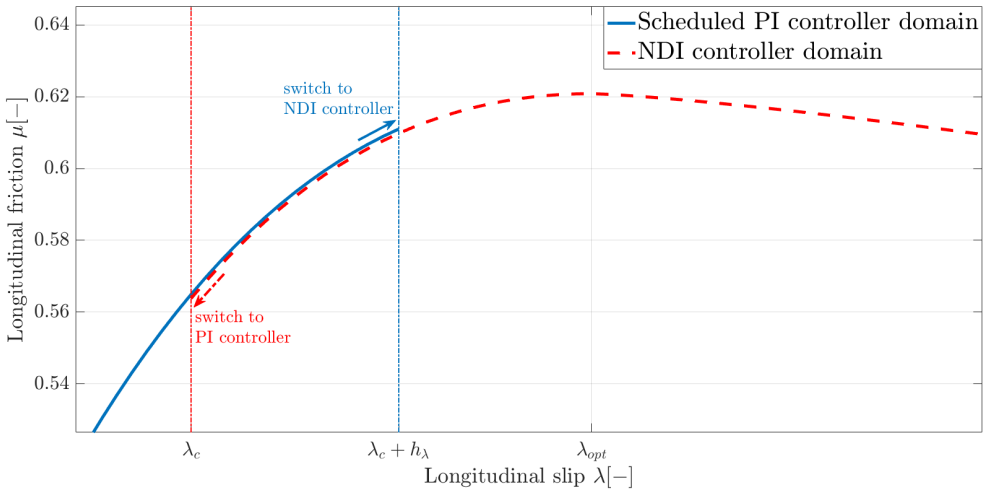

Figure 7: Switching strategy and resulting controller operating domains

More precisely, as clarified next, the switching strategy is implemented to enforce continuity of the commanded braking torque.
Let us denote t_k and t_{k+1} two successive switching times where by convention $t_0 = 0\ s$ is the initial time. Then, in each interval $[t_k,\ t_{k+1}]$, the control law is either defined by the implicitely time-varying PI based structure:

$$u(t) = u_{PI}(t) = u(t_k) + K_p\,(v) \cdot (\lambda_c - \lambda) + \int_{t_k}^{t} K_i\,(\lambda)\,(\lambda_c - \lambda)\ d\tau \tag{38}$$

or by the NDI-based explicitely time-varying expression:

DOI: 10.13009/EUCASS2022-4404

$$u(t) = u_{TV}(t) = T\left(u(t_k), \hat{\Psi}(t)\right) - K(v) \cdot (t - t_k) \tag{39}$$

where $T(c, s(t))$ denotes a smooth transition operator from the constant first input argument $c = u(t_k)$ to the varying signal $s(t) = \hat{\Psi}(t)$. This operator will then guarantee the continuity of the commanded torque when switching occurs from (38) to (39) with t_k such that $\lambda(t_k) = \lambda_c + h_\lambda$. Next, note that switches from law (39) to (38) take place when $\lambda(t_k) = \lambda_c$, in which case $u_{PI}(t_k) = u(t_k)$ and continuity is then enforced.

Remark. *During normal operations in practice, it is observed that* $u(t_k) \approx \hat{\Psi}(t_k)$ *so that the transition operator can be removed to recover equation* (37) *without significant impact on the global behavior.*

4. Estimation

The present section deals with the estimation of the key variables of the problem.

An extended state observer able to estimate the nonlinear grip moment $\Psi(\lambda)$, only from wheel speed measurement and commanded torque, is first presented. This estimate is used not only to generate the control signal when the NDI controller is active (see (39)), but also to derive estimates of the aircraft speed v and controlled variable λ.

4.1 Extended State Observer for grip moment estimation

Consider the nonlinear system of (7), neglecting the longitudinal velocity variations compared to the slip dynamics. The system can be rendered linear by considering the grip moment $\Psi(\lambda)$, which contains the nonlinearity, as a second state variable, whose variations are neglected:

$$\begin{cases} \begin{bmatrix} \dot{\omega} \\ \dot{\Psi} \end{bmatrix} = \begin{bmatrix} 0 & \frac{1}{J} \\ 0 & 0 \end{bmatrix} \begin{bmatrix} \omega \\ \Psi \end{bmatrix} + \begin{bmatrix} -\frac{1}{J} \\ 0 \end{bmatrix} T_b \\ \omega = \begin{bmatrix} 1 & 0 \end{bmatrix} \begin{bmatrix} \omega \\ \Psi \end{bmatrix} \end{cases} \tag{40}$$

Note that the wheel speed ω is measured, while the applied braking torque is not generally directly available. Based on the above, an observer can be implemented as followed:

$$\begin{cases} \dot{\hat{X}} = A\,\hat{X} + B\,T_c + L\,(\omega_m - \hat{\omega}) \\ \hat{\omega} = C\,\hat{X} \end{cases} \tag{41}$$

where $\hat{X} = \begin{bmatrix} \hat{\omega} \\ \hat{\Psi} \end{bmatrix}$ is the state vector estimate, $L = \begin{bmatrix} L_1 \\ L_2 \end{bmatrix}$ is the observer gain matrix, $A = \begin{bmatrix} 0 & \frac{1}{J} \\ 0 & 0 \end{bmatrix}$, $B = \begin{bmatrix} -\frac{1}{J} \\ 0 \end{bmatrix}$ and $C = [1 \quad 0]$. The inputs are the wheel speed measurement ω_m and commanded torque T_c.

The gains $L_1 = 40$ and $L_2 = 800 \times J$ are retained so as to ensure the observer convergence with a bandwidth $\omega_{obs} \approx 28 rad/s$.

The grip moment estimate $\hat{\Psi}$ returned by the observer is used by the NDI controller operating in the unstable region of the friction curve (see (39)) but also in the following subsection to reconstruct the wheel slip λ.

4.2 Wheel slip estimation

Taking into consideration the entire aircraft, on which the aerodynamic drag $D = -k_d v^2$ is not negligible, (5b) can be rewritten:

$$\dot{v} = \frac{D}{m_{tot}} - \frac{1}{m_{tot}} \sum_{i=1}^{n} F_{x_i} = -\frac{k_d}{m_{tot}} v^2 - \frac{1}{r\, m_{tot}} \sum_{i=1}^{n} \Psi_i \tag{42}$$

where n is the number of braked wheels (supposed of same rolling radius r), Ψ_i, F_{x_i} are respectively the grip moment and longitudinal force of the i^{th} wheel. m_{tot} is the aircraft total mass, while k_d is the coefficient verifying $D = -k_d v^2$.

From $\hat{\Psi}$ and (42), an estimate of the longitudinal acceleration can be deduced as:

$$\dot{\hat{v}} = -\frac{k_d}{m_{tot}} v^2 - \frac{1}{r\, m_{tot}} \sum_{i=1}^{n} \hat{\Psi}_i \tag{43}$$

DOI: 10.13009/EUCASS2022-4404

which, via integration, leads to the longitudinal velocity estimate as in (44), provided the initial value of the aircraft v_0 is known. The latter can be estimated accurately from the initial values of the wheel speed as $v_0 = \underset{1\leq i\leq n}{max}\Big(r\,\omega_{m_i}(0)\Big)$, given that the slip is null prior to braking.

$$\hat{v}(t) = v_0 - \frac{1}{m_{tot}}\int_0^t k_d v(\tau)^2 - \frac{1}{r}\sum_{i=1}^{n}\hat{\Psi}_i(\tau)\,d\tau \tag{44}$$

Finally, each wheel slip λ_i is estimated as:

$$\hat{\lambda}_i = 1 - \frac{r\,\omega_{m_i}}{\hat{v}} \tag{45}$$

Remark. *The aircraft aerodynamic constant k_d was assumed to be known. A satisfying estimate can be obtained through the wheel speed measurements just before the brake torque is applied according to the following:*

$$k_d = \frac{m_{tot}\,r}{v_0^2}\,\hat{\dot{\omega}}_0 = \frac{m_{tot}}{r\,\underset{1\leq i\leq n}{max}\Big(\omega_{m_i}(0)\Big)^2}\,\hat{\dot{\omega}}_0 \tag{46}$$

where $\hat{\dot{\omega}}_0$ is an estimate of the wheel deceleration obtainable from the speedometer measurements on a sufficiently long time horizon (e.g. $10\,T_s$).

5. Simulation results

In this section, the complete braking control architecture is tested via simulation on the high-fidelity aircraft on-ground model presented in Ndiaye et al.[16]

5.1 Validation model and test scenarios

The nonlinear 6 degrees-of-freedom aircraft model considered offers a reliable simulation environment for braking control validation by incorporating longitudinal-vertical cross-coupling phenomena typical of braking. In particular, the behavior of the shock-absorbers is particularly well described which allows to depict accurately the wheels rolling radii variations and the resulting effects on the wheel slip and friction forces. The model is supplemented with the servo-valve second order dynamics (11) and the model for speedometer delay (12). The resulting overall tractable model provides precise simulation results used to validate the proposed braking control scheme. The set of data, corresponding to a single-aisle aircraft, available in Ndiaye et al[16] are used for the simulations.

Besides aircraft stopping distance, the following meaningful performance criterion is used to assess the braking efficiency:

$$e_{\%} = 100\frac{\int_{t_i}^{t_f}\mu\Big(\lambda\,(t)\Big)dt}{\int_{t_i}^{t_f}\mu_{max}\,(t)\,dt} \tag{47}$$

where μ_{max} is the maximum friction available at the tire/runway interface, t_i and t_f are the braking process initial and final times.

The proposed slip control architecture is assessed on two Rejected takeoff (RTO) braking maneuvers occurring on two different runways:

1. A homogeneous dry runway.
2. A heterogeneous runway characterized by a sudden transition from dry to very wet condition, the associated μ-discontinuity occurring 220 m after braking initiation.

During an RTO, the takeoff process is aborted due to an unexpected hazardous event and the aircraft has to be stopped safely within the remaining length of runway available. In such a critical situation, the objective is clearly to continuously exploit a maximum amount of the friction available at the runway in order to generate the minimum braking distance. In both scenarios, the aircraft speed is initialized at the takeoff decision speed $v_1 = 70\ m/s$.

The first maneuver aims at assessing the ability to generate an optimal steady high-performance braking in the nominal configuration corresponding to a homogeneous dry runway. In the specific proposed scenario, the large negative friction curve slope of the unstable region, typical of dry runways (see Figure 2), has the propensity to cause

DOI: 10.13009/EUCASS2022-4404

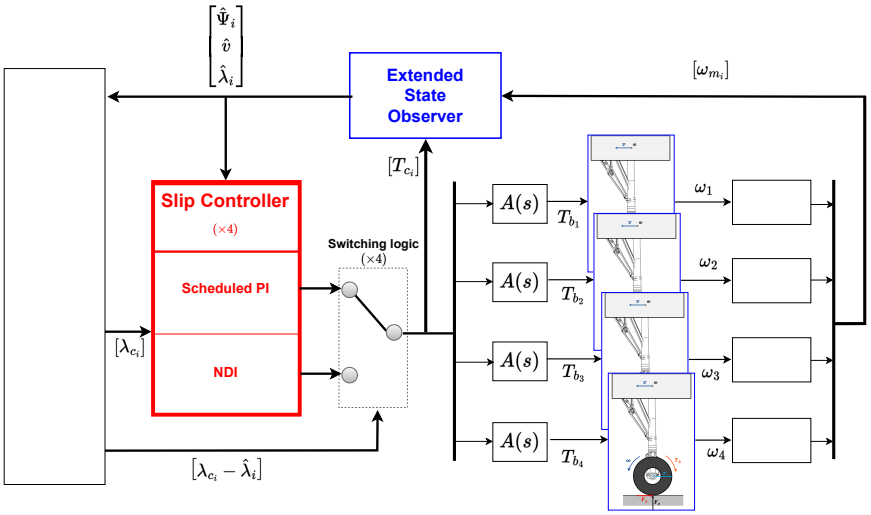

Figure 8: Overall braking control architecture (the braking supervisor logic is not detailed in the present paper)

profound wheel skids. As a result, the scenario tends to disadvantage suboptimal overaggressive antiskid systems. By the second scenario, the objective is to test the adaptation to a drastic change in friction coefficient, due to a puddle *e.g.*, during a hard braking process. Moreover, the wet runway section is characterized by a lower friction coefficient μ with moderate slope values above the peak (see Figure 2). Such a configuration is likely to handicap too conservative braking control systems. The combination of both scenarios is relevant to validate the performance, robustness and versatility of the braking control architecture. Remark that both maneuvers are perfectly symmetrical, *i.e.* no crosswind, a same runway condition experienced by right and left landing gear wheels as well as a single slip reference signal for all the wheels are assumed.

5.2 Results analysis

The simulations results of the homogeneous and heterogeneous braking scenarios appear in Figures 9 and 10 respectively. Regarding the first scenario, to assess the efficiency of the controller switching strategy, the results obtained with and without the hysteretic commutation (see section 3.3) are displayed for both the single wheel synthesis model (introduced in section 2.1) and the complete aircraft validation model. In particular, the aircraft and wheel speeds as well as the reference, realized and estimated wheel slips, are represented for each of the four cases in Figures 9a - 9h. The evolution of the reference and realized slips allows to study the overall tracking ability of the control scheme. The observer performance can be more specifically assessed through the results of the heterogeneous braking, which corresponds to the worst case regarding estimates accuracy. Therefore, the realized and estimated aircraft speed and wheel grip moment are also depicted for the second scenario, see Figures 10c and 10d respectively. Note that for the validation model, the results correspond to only one of the four landing gear wheels, the other wheels producing exactly the same results since both maneuvers are symmetrical. The slip setpoint variations observed in simulations result from the braking supervisor logic, not detailed here.

Regarding the controllers commutation, Figure 9 shows that the hysteretic switching strategy allows to achieve a better tracking of the slip setpoint signal by reducing the activation time of the NDI controller, whose activation state (1 for activated, 0 for inactivated) is displayed at the bottom of the wheel slip plots in Figures 9b, 9d, 9f and 9h. When no hysteresis switching is applied, unwanted commutations are observed on both the synthesis and validation models. Despite its first order dynamics (10), the single wheel model slip response incurs overshoots and consequent controller commutations as a result of the slip estimate discrepancy, see Figure 9b. For the validation model, the overshoots result from the landing gear vertical dynamics, *i.e.* variations of the wheel rolling radius r and vertical load F_z, that produces noticeable oscillations on the wheel slip response, as can be seen in Figure 9h. The value $h_\lambda = 0.03$ defined in design is sufficient to maintain the wheel slip in the PI controller operating domain without unnecessary activation of the NDI

DOI: 10.13009/EUCASS2022-4404

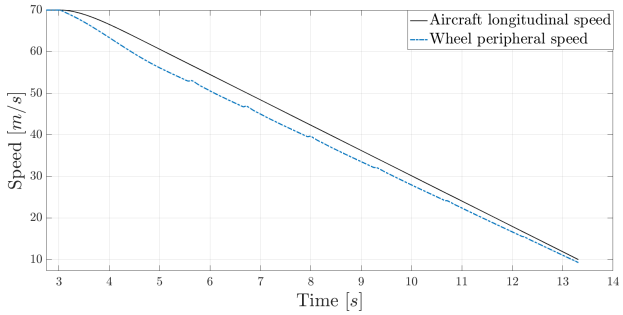

(a) Synthesis model (without hysteresis): Aircraft and wheel speeds

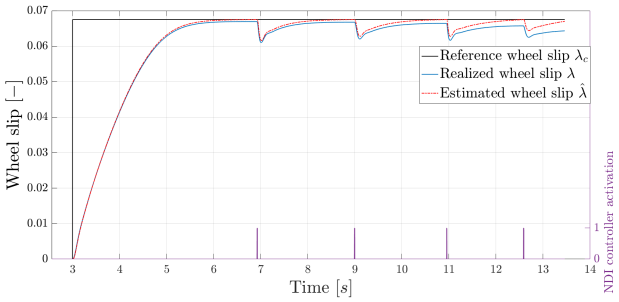

(b) Synthesis model (without hysteresis): Wheel slip control and estimation performance

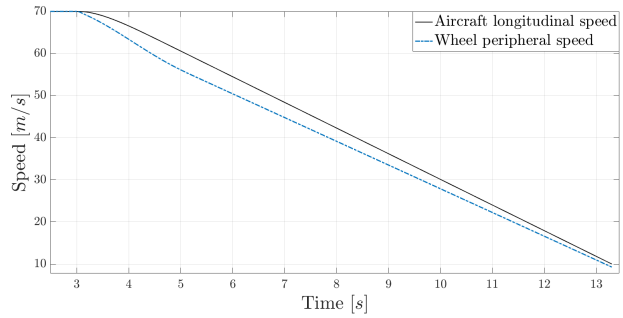

(c) Synthesis model (with hysteresis): Aircraft and wheel speeds

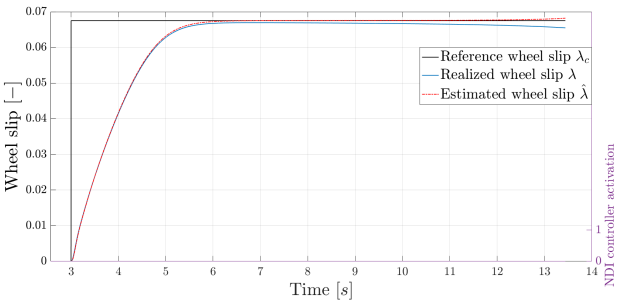

(d) Synthesis model (with hysteresis): Wheel slip control and estimation performance

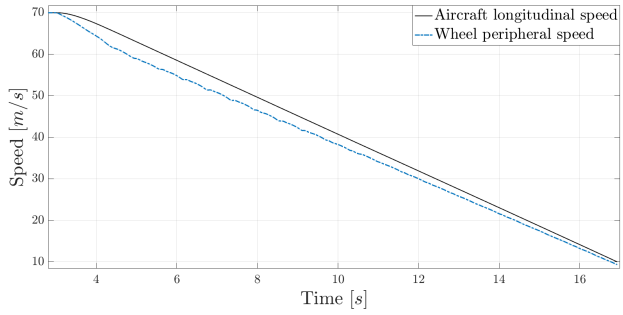

(e) Validation model (without hysteresis): Aircraft and wheel speeds

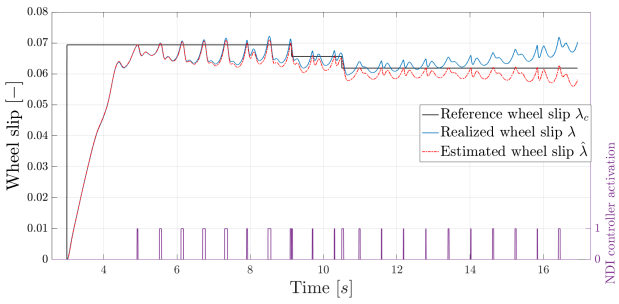

(f) Validation model (without hysteresis): Wheel slip control and estimation performance

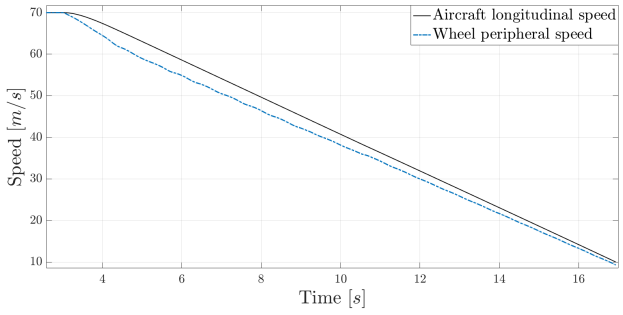

(g) Validation model (with hysteresis): Aircraft and wheel speeds

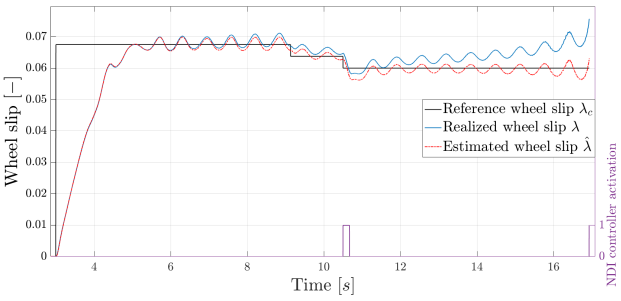

(h) Validation model (with hysteresis): Wheel slip control and estimation performance

Figure 9: Dry runway RTO: effects of hysteretic switching on single wheel and complete aircraft validation models

DOI: 10.13009/EUCASS2022-4404

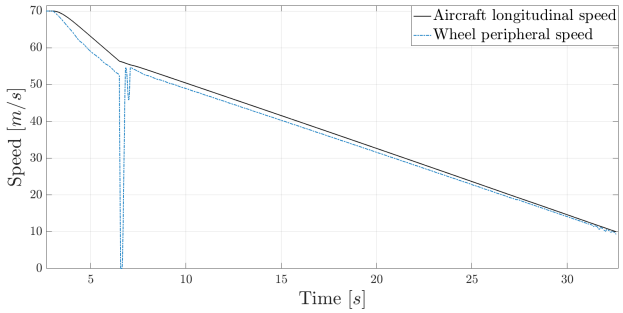

(a) Aircraft and wheel speeds

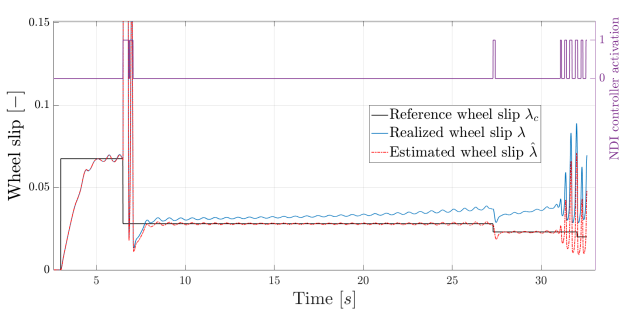

(b) Wheel slip control and estimation performance

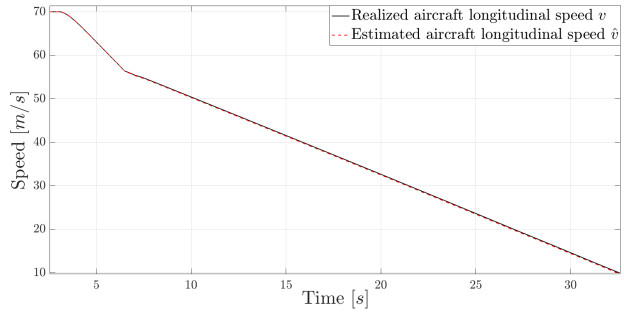

(c) Aircraft longitudinal speed: realized and estimated

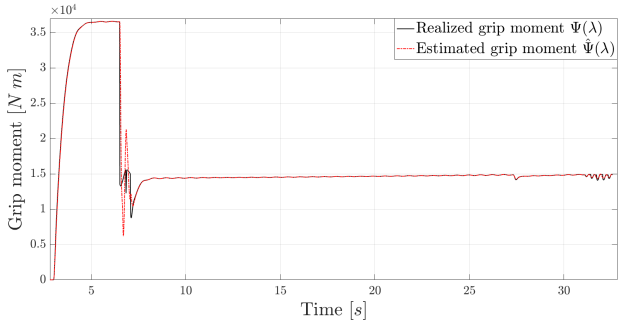

(d) Wheel grip moment: realized and estimated

Figure 10: Braking on a heterogeneous runway, from dry to wet, with $\mu-$discontinuity at $6.5s$ (results corresponding to a right landing gear wheel)

controller, see Figures 9d and 9h.

As far as the homogeneous braking performance is concerned, Figures 9g and 9h show that the proposed control law allows to track the reference wheel slip without any excessive overshoot. The estimated wheel slip signal, used in the closed loop by the controller, satisfactorily follows the realized slip in spite of an increasing mismatch over time.

With regard to the heterogeneous braking, the transition from a dry to a very wet portion provokes a short-lived wheel lock as depicted in Figures 10a and 10b. However, this wheel lock remains limited in time ($< 0.1\ s$) and was almost inevitable regarding the differences in friction for the dry and wet conditions used in simulation (see Figure 2). We can notice that for a moderate slip setpoint value on the wet runway section ($\lambda_c \approx 0.75\ \lambda_{opt}$), the slip response oscillations are reduced. The unstable region NDI controller remains inactive during most of the braking process. Meanwhile, the realized friction stays very high ($\mu \approx 0.95\ \mu_{max}$). Nevertheless, the slip estimation error is more important than for the first scenario at the end of the simulation. This can be explained by the longer deceleration occurring on the wet runway, which leads to a larger cumulated error. The reduced realized slip values achieved on the wet runway tend to amplify the relative estimation error $\left(e_\lambda = \frac{\hat{\lambda}-\lambda}{\lambda}\right)$ as well. This discrepancy between the actual and estimated slips being negative ($e_\lambda < 0$) and the setpoint λ_c being relatively near the optimum λ_{opt} during an RTO, the realized slip λ becomes repeatedly greater than λ_{opt} and skids are incurred from $t = 31\ s$. While limited ($\lambda < 0.1$), these wheel skids activate the NDI controller when they are detected by the commutation logic (*i.e.* when $\hat{\lambda} \geq \lambda_c + h_\lambda$) and a recurring switching is observed accordingly.

Table 1: scenarios performances results

	Dry runway*	**Heterogeneous runway**
$e_{\%}$ [%]	95.67	94.51
Realized braking distance [m]	571	1095
Minimum braking distance attainable [m]	535	1000

* *Results obtained with the hysteretic commutation logic*

Despite severe conditions imposed by the two braking scenarios, the wheel slip control architecture herein proposed demonstrates ability to satisfactorily track the reference input and generate very efficient braking as shown in Table 1. As a result, the braking distances remain very close to the theoretical minimum attainable values. Room for

DOI: 10.13009/EUCASS2022-4404

improvement should be sought in ways to mitigate chattering effect due to the switching process while still ensuring the unstable region is left when crossed into. Even though the observer is very accurate in estimating v and Ψ, the reconstruction of λ generates a potentially hazardous mismatch regarding closed-loop stability at the end of a long braking process and for low slip values. Note that the simulations were performed until the aircraft velocity attains the critical value of 10 $m\ s$, below which an open-loop braking is assumed to be safe enough regarding skid induced tire blowout risks.

6. Conclusion and future work

An efficient aircraft braking control architecture is presented and tested on a reliable and validated simulation environment. The main constraints typical of aeronautics, such as actuator bandwidth, sensor delays or limited measurements available, are considered in design and validation. The wheel slip control law relies on the combination of a gain-scheduled PI controller, achieving high-performance tracking in the stable region, together with a NDI controller guaranteeing efficient leaving of the friction curve unstable domain. The controllers are provided by accurate estimations of the grip moment, aircraft velocity and of the controlled variable λ. Such an exhaustive approach allows a successful adaptation to the vast operating conditions. The estimates are realized by means of an extended state observer which directly considers the nonlinearity as part of a state variable, alleviating the potential mismatch introduced otherwise by linearization. The advanced validation of the overall architecture demonstrated stability, which substantiate the benefits of wheel slip control applied to aircraft braking. The evolution of the wheel slip estimate error over long braking processes, however, together with ways to reduce chattering without compromising the ability to leave the unstable domain, must be further investigated. Future work will also focus on studying strategies to identify λ_{opt} and update the setpoint λ_c accordingly[21,22] .

References

[1] L. D'Avico, M. Tanelli, S.M. Savaresi, M. Airoldi, and G. Rapicano. A deceleration-based algorithm for anti-skid control of aircraft. *IFAC-PapersOnLine*, 50(1):14168–14173, 2017. 20th IFAC World Congress.

[2] M.A. Lonbani, M. Morandini, P. Astori, and G. Ghiringhelli. Anti-skid braking control system design for aircraft: Multi-phase schemes approach. In *2017 5th IEEE International Conference on Models and Technologies for Intelligent Transportation Systems (MT-ITS)*, pages 104–109, 2017.

[3] S. Savaresi and M. Tanelli. *Active Braking Control Systems Design for Vehicles*. Springer, 01 2011.

[4] T.A. Johansen, I. Petersen, J. Kalkkuhl, and J. Ludemann. Gain-scheduled wheel slip control in automotive brake systems. *IEEE Transactions on Control Systems Technology*, 11(6):799–811, 2003.

[5] G. Papa, V. Breschi, M. Tanelli, S. Formentin, and S.M. Savaresi. Direct data-driven lpv control for active braking in aircraft. *IFAC-PapersOnLine*, 54(8):116–123, 2021. 4th IFAC Workshop on Linear Parameter Varying Systems LPVS 2021.

[6] F Courbun and M Cassaro. Method and device for assisting piloting of an aircraft moving on the ground, December 30 2021. US Patent App. 17/358,352.

[7] F Villaume, A Jacob, and R Lignee. Method and device to assist in the piloting of an aircraft in a landing phase, 2008. US8209072B2.

[8] G. Papa, M. Tanelli, G. Panzani, and S.M. Savaresi. Wheel-slip estimation for advanced braking controllers in aircraft: Model based vs. black-box approaches. *Control Engineering Practice*, 117:104950, 2021.

[9] Sergey V. Drakunov, Ümit Özgüner, Peter Dix, and Behrouz Ashrafi. Abs control using optimum search via sliding modes. *IEEE Trans. Control. Syst. Technol.*, 3:79–85, 1995.

[10] M. Tanelli, A. Ferrara, and P. Giani. Combined vehicle velocity and tire-road friction estimation via sliding mode observers. In *2012 IEEE International Conference on Control Applications*, pages 130–135, 2012.

[11] M.Q. Chen, W.S. Liu, Y.Z. Ma, J. Wang, F.R. Xu, and Y.J. Wang. Mixed slip-deceleration pid control of aircraft wheel braking system. *IFAC-PapersOnLine*, 51(4):160–165, 2018. 3rd IFAC Conference on Advances in Proportional-Integral-Derivative Control PID 2018.

DOI: 10.13009/EUCASS2022-4404

[12] L. D'Avico, M. Tanelli, S.M. Savaresi, M. Airoldi, and G. Rapicano. An anti-skid braking system for aircraft via mixed-slip-deceleration control and sliding mode observer. In *2017 IEEE 56th Annual Conference on Decision and Control (CDC)*, pages 4503–4508, 2017.

[13] I. Tunay, M. Amin, E. Rodin, American Institute of Aeronautics, and Astronautics. Neural network augmented anti-skid controller for transport aircraft. 1999.

[14] H.C. Tseng and C.W. Chi. Aircraft antilock brake system with neural networks and fuzzy logic. *Journal of Guidance Control and Dynamics*, 18:1113–1118, 1995.

[15] A. Jacquet, Y. Chamaillard, M. Basset, G. Gissinger, D. Frank, and J.P. Garcia. Anti-lock braking system using predictive control and on-line tire/road characteristics estimation. *IFAC Proceedings Volumes*, 41(2):2099–2104, 2008. 17th IFAC World Congress.

[16] A.W. Ndiaye, M. Cassaro, J-M. Biannic, C. Combier, and C. Roos. On-ground aircraft modeling for advanced braking control system design. In *Proceedings of the European Control Conference*, 2022.

[17] H.B. Pacejka. *Tire and Vehicle Dynamics*. 01 2006.

[18] R Castro, R Araújo, M Tanelli, S Savaresi, and D Freitas. Torque blending and wheel slip control in evs with in-wheel motors. *Vehicle System Dynamics - VEH SYST DYN*, 50:71–94, 01 2012.

[19] R. Poley. Dsp control of electro-hydraulic servo actuators. 2005.

[20] R.H. Brown, S.C. Schneider, and M.G. Mulligan. Analysis of algorithms for velocity estimation from discrete position versus time data. *IEEE Transactions on Industrial Electronics*, 39(1):11–19, 1992.

[21] R Castro, R Araújo, and D Freitas. Real-time estimation of tyre-road friction peak with optimal linear parameterisation. *Control Theory and Applications, IET*, 6:2257–2268, 09 2012.

[22] A Albinsson. *Online and offline identification of Tyre model parameters*. Chalmers Tekniska Hogskola (Sweden), 2018.